

pubs.acs.org/Macromolecules Article

Viscoelastic Response of Dispersed Entangled Polymer Melts

Brandon L. Peters, K. Michael Salerno, Ting Ge, Dvora Perahia, and Gary S. Grest*



Cite This: Macromolecules 2020, 53, 8400-8405

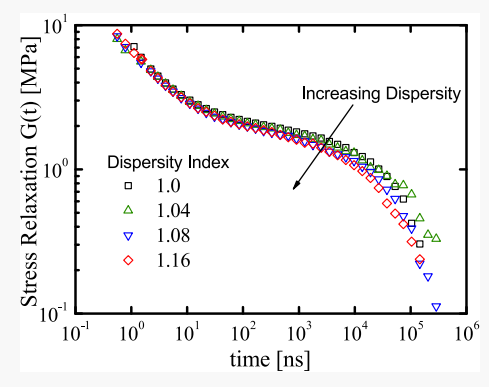


ACCESS

III Metrics & More

Article Recommendations

ABSTRACT: Polymer synthesis routes result in macromolecules with molecular weight dispersity $D_{\rm M}$ that depends on the polymerization mechanism. The lowest dispersity polymers are those made by anionic and atom-transfer radical polymerization, which exhibit narrow distributions $D_{\rm M} = M_{\rm w}/M_{\rm n} \sim 1.02-1.04$. Even for small dispersity, the chain length can vary by a factor of two from the average. The impact of chain length dispersity on the viscoelastic response remains an open question. Here, the effects of dispersity on stress relaxation and shear viscosity of entangled polyethylene melts are studied using molecular dynamics simulations. Melts with chain length dispersity, which follow a Schulz–Zimm (SZ) distribution with $D_{\rm M} = 1.0-1.16$, are studied for times up to 800 μ s, longer than the terminal time. These systems are compared to those with binary and ternary distributions. The stress relaxation functions are extracted from the Green–Kubo relation and from stress relaxation following a uniaxial extension. At short and



intermediate time scales, both the mean squared displacement and the stress relaxation function G(t) are independent of $D_{\rm M}$. At longer times, the terminal relaxation time decreases with increasing $D_{\rm M}$. In this time range, the faster motion of the shorter chains results in constraint release for the longer chains.

■ INTRODUCTION

Dispersity in polymers' molecular weight is inherent to the statistical nature of their synthesis routes, where variability in chain lengths results in a different number average molecular weight M_n and weight average molecular weight M_w . The degree of dispersity is defined as $D_{\rm M} = M_{\rm w}/M_{\rm n}$. The lowest dispersity is found in anionic and atom-transfer polymerization^{2,3} in which \mathcal{D}_{M} is of the order of 1.02–1.04. For most commodity polymers, \mathcal{D}_{M} is significantly higher, which strongly influences mechanical and rheological responses. As we have previously shown, even dispersity as small as $D_{\rm M} = 1.02-1.04$ is sufficient to affect the chain mobility.4 The current study probes the effects of low dispersity on the stress relaxation at the crossover from ideal monodispersed polymers to realistic ones. Through fine tuning of dispersity, we show that dispersity increases the mobility of the long chains relative to long chains in a monodispersed melt of a similar chain length. This, in turn, leads to a decrease in the time required to fully relax the stress in polymer melts.

Experimentally, Graessley and co-workers have shown that the viscoelastic response of a polymer melt is highly sensitive to chain dispersity, particularly for high molecular weights. However, following the effect of $\mathcal{D}_{\rm M}$ on the relaxation of individual chains remains a challenge experimentally. Theoretically, dispersed melts have mainly been treated by extending models of monodispersed melts to include chain length dispersity. These studies have largely focused on linear viscoelasticity of entangled polymer melts $^{8-16}$ and clearly

demonstrate that the dynamics of linear chains in dispersed polymeric melts cannot be described solely by classical reptation theory.

Computations enable a systematic study of the effects of dispersity in polymer chain length on viscoelastic response. However, to capture the viscoelastic response for polymers with dispersity correctly, especially in the entangled regime, requires probing large systems for long times. Therefore most numerical simulations have largely focused on monodispersed $(D_{\rm M}=1)$ systems. Dispersed systems have mostly been modeled by blends of two chain lengths, $^{17-23}$ with only a few studies of polymer melts with a distribution of chain lengths. 17,24-32 Rorrer and Drogan studied entangled melts using a lattice dynamic Monte Carlo method with three unique chain lengths to represent different degrees of dispersity. Recently, we directly probed the mobility of dispersed entangled polymer melts with distribution as narrow as experimentally attainable for long entangled polymers. 4 We showed that while the average diffusion constant of the chains increases weakly with increasing $D_{\rm M}$, the mobility of the shortest and longest chains deviate considerably from the

Received: June 16, 2020
Revised: September 10, 2020
Published: October 1, 2020





average. This enhanced diffusion of the shorter chains results in constraint release for the longer chains, leading to a faster motion of the long chains than in a monodispersed melt of long chains. Building on our previous study of chain mobility for narrow distributions of molecular weight, we resolve the effects of low chain length dispersion on the stress relaxation and shear viscosity. Understanding this low dispersity regime opens the way to evaluate the degree of dispersity that affects mechanical properties.

Using a coarse grained (CG) model for polyethylene (PE) with four methylene groups per CG bead, $^{33-35}$ we examine stress relaxation of dispersed entangled polymer melts with dispersity $\mathcal{D}_{\rm M}$ and compare the results to a monodispersed polymer melt. This CG model was shown 33,34 to capture both the structure and dynamics of uniform PE melts. Here, we compare the chain mobility, stress relaxation, and shear viscosity for a Schulz–Zimm (SZ) distribution of molecular weights, $^{1,36,37}_{,37}$ with binary and ternary distributions with the same weight averaged molecular weight $M_{\rm w}$. The Schulz–Zimm distribution describes the molecular weight distribution of polymer melts synthesized by anionic and atom-transfer radical polymerization. We focus on low dispersity $(1.0 \leq \mathcal{D}_{\rm M} \leq 1.16)$ to match the optimal synthesis routes for attaining the lowest possible $\mathcal{D}_{\rm M}$ experimentally.

MODEL AND METHODS

The current study uses a CG model with four methylene groups per CG bead. 33,35,38 This CG scheme is chosen since for more than five methylene groups per bead, additional constraints are needed to prevent chains from crossing. 33,34,39,40 This CG potential was previously derived from an atomistic simulation of $C_{96}H_{194}^{33,34}$ at T=500 K and density 0.76 g/cm³ using an iterative Boltzmann procedure with pressure corrections.^{33,34} The atomistic simulations used the Optimized Potentials for Liquid Simulations (OPLS) force fields of Jorgensen et al. 41,42 potential with modified dihedral coefficients to better reproduce the properties of long alkanes. 43 A tabulated CG angle and bond potentials were determined by Boltzmann inversion of the atomistic bond and angle distributions. Torsion CG terms were omitted. The detailed description of the CG development is given by Salerno et al.^{33,38} and Peters et al.³⁵ For the monodispersed system studied here, the mean squared end-to-end distance $\langle R^2 \rangle / M_w = 1.31 \text{ Å}^2 \text{ mol/g}$, which is in very good agreement with the experimental value of 1.25 Å² mol/g for polyethylene at 413 K was determined from small-angle neutron scattering.⁴⁴ The packing length was p = 1.8 Å compared to the experimental value of p = 1.69 Å at 413 K.⁴⁴

To model the distributions of chain lengths, we used the Schulz–Zimm distribution 1,36,37 that commonly captures the length distribution in chromatography with $D_{\rm M}=1.0-1.16$ and $M_{\rm w}=35.8~{\rm kg/mol.^4}$ This corresponds to 2560 CH₂ monomers or 640 CG beads per chain for the monodispersed system. For comparison, we also studied binary and ternary blends with $D_{\rm M}=1.04$, as shown in Figure 1. Experimentally, the entanglement molecular weight for PE is $M_{\rm e}\sim1.1-1.2~{\rm kg/mol.^{45,46}}$ which corresponds to about 20 CG beads. Using this experimental value for M_e , the number of entanglements per chain $Z=M_{\rm w}/M_{\rm e}\sim30-33$. To represent the Schulz–Zimm distribution, one melt of $N_{\rm c}=2000$ chains was studied for 1.02 $\leq D_{\rm M} \leq 1.08$ and $N_{\rm c}=4000$ chains for $D_{\rm M}=1.16$. There are 398, 524, 671, and 940 unique chain lengths for $D_{\rm M}=1.02$, 1.04, 1.08, and 1.16 respectively. For the largest dispersity $D_{\rm M}$

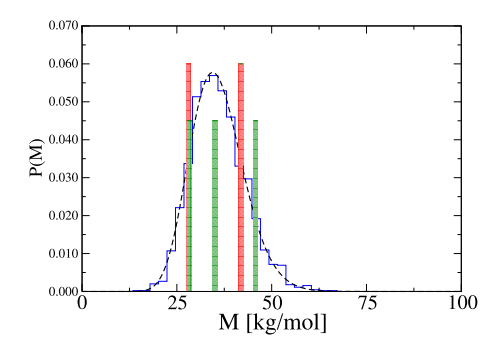


Figure 1. Chain length distribution P(M) versus molecular weight M for $D_{\rm M}=1.04$. Results for our system of 2000 chains (blue) are compared to the analytic Schulz–Zimm formula (black). Results for binary (red) and ternary (green) distributions with $D_{\rm M}=1.04$ are also shown for arbitrary weight to fit on the graph.

= 1.16, the chains range in length from 94 to 1834 CG beads. For $\mathcal{D}_{\rm M}$ = 1.0, two systems of $N_{\rm c}$ = 1000 chains were studied. The binary system contained 1000 chains of M = 41.3 kg/mol and 1000 chains of 27.6 kg/mol. The tertiary system contained 666 chains of M = 45.3, 34.5, and 27.9 kg/mol each.

Simulations were performed using the Large Atomic Molecular Massive Parallel Simulator (LAMMPS) molecular dynamics code with a time step of 20 ps. The chains were built following the procedure described by Auhl et al. With periodic boundary conditions. All simulations were run at a constant density $\rho=0.76$ g/cm³ and temperature T=500 K. A Langevin thermostat with a weak damping constant of 100 ps was applied to maintain the temperature.

Coarse graining reduces the number of degrees of freedom, creating a smoother free-energy landscape compared with fully atomistic simulations. This results in faster dynamics for the CG polymer chain than for the fully atomistic model. 49-52 To overlay the mean squared displacement (MSD) of the chains from the atomistic and CG simulations, time in the CG simulations is scaled by a temperature-dependent, dimensionless dynamic scaling factor α . For the current model at T = 500K, $\alpha = 6.2^{33,38}$ In all of the results presented here, time was scaled by α . The systems studied were run for $4.0-6.8 \times 10^9$ time steps or the equivalent of 496-840 µs. All results presented here are for the weight averaged MSD. All simulations were run on Sandia's computer clusters. A billion time steps took 430 or 900 h or between 0.75 and 1.5 millioncore h for the 2000 chain systems (1.02 $\leq D_{\rm M} \leq$ 1.08) depending on the specific cluster and number of nodes used. For the 4000 chain, $D_{\rm M}$ = 1.16 system, a billion steps took 800 h on our fastest cluster. The actual time to complete the runs is two to three times longer.

The stress relaxation modulus G(t) was measured for each system using the Green–Kubo relation $G(t) = (V/k_BT)$ $\langle \sigma_{\alpha\beta}(t)\sigma_{\alpha\beta}(0)\rangle$, where $\sigma_{\alpha\beta}(t)$ are the off-diagonal components xy, xz, and yz of the stress and V is the volume. The normal stress decay after deforming polymer chains in a melt by a small step strain was also measured. This was done by deforming the system by an elongation λ in the x-direction $L_x = \lambda L$ while shrinking the simulation cell in the other two directions $L_y = L_z = L/\sqrt{(\lambda)}$ to keep the density of the system constant. Using the stress–strain description for classical rubber elasticity, 54 G(t) is given by

$$G(t) = \frac{\sigma_{xx}(t) - \frac{1}{2}(\sigma_{yy}(t) + \sigma_{zz}(t))}{\lambda^2 - \frac{1}{\lambda}}$$
(1)

Here, we use $\lambda = 1.2$ following Hsu and Kremer,⁵³ who applied this method to determine G(t) for the standard bead spring model.⁵⁵

Nonequilibrium MD simulations were carried out to measure the shear viscosity η as a function of the shear rate. We integrate the SLLOD (which adopts the transpose of the qp-DOLLS tensor⁵⁶) equations of motion^{57,58} with a damping constant of 1 ps (unscaled). The shear viscosity is calculated using $\eta = -\sigma_{xz}/\dot{\gamma}$, where σ_{xz} is the xz component of stress along the flow and gradient directions, respectively, and $\dot{\gamma}$ is the strain rate. After an initial overshoot, σ_{xz} reaches a plateau for $\dot{\gamma}t\gg 1$. This plateau is used to estimate the shear viscosity η . Note that including the dimensionless scaling factor α decreases the effective shear rate $\dot{\gamma}$ and increases the effective viscosity η compared to the unscaled values.³⁸

RESULTS

The mean squared displacement of the center of mass $g_3(t) = \langle (r_{\rm cm}(t) - r_{\rm cm}(0)) \rangle^2$ and the center four CG beads of the chain $g_1(t) = \langle (r_i(t) - r_i(0)) \rangle^2$ for the Schulz–Zimm, binary, and ternary distributions with the $M_{\rm w}=35.8$ kg/mol and $D_{\rm M}=1.04$ are shown in Figure 2. These results show that for a fixed

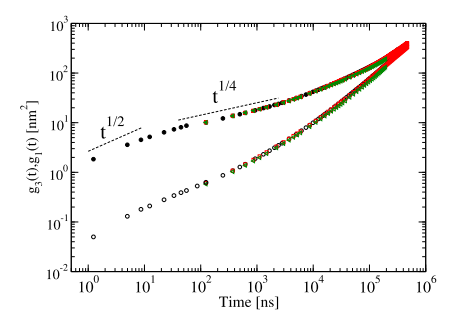


Figure 2. Weight averaged mean squared displacement of the center of mass $g_3(t)$ (open) and center four CG beads $g_1(t)$ (solid) for Schulz–Zimm (black), binary (red), and (green) tertiary with $D_{\rm M}=1.04$.

dispersity, the mobility of the chains and the monomers do not depend on the functional form (Shulz–Zimm, binary, or ternary) of the distribution, at least for small dispersity. From the crossover in $g_1(t)$ from the early Rouse relaxation $t^{1/2}$ regime to the $t^{1/4}$ reptation regime, we estimate the tube diameter $d_{\rm T}$ and entanglement time $\tau_{\rm e}$. From the results shown in Figure 2, the crossover time $t_{\rm e}^* \sim 14$ ns and $g_1(t_{\rm e}^*) \sim 4.9$ nm². Assuming that the distribution of segment displacement along the tube is Gaussian on the scale of the tube diameter $d_{\rm T}$, the entanglement time $\tau_{\rm e} = (9/\pi)t_{\rm e}^* \sim 40$ ns and tube diameter $d_{\rm T} = \sqrt{(3\pi/2)g_1(t_{\rm e}^*)} \sim 4.8$ nm. At these early times, the results are consistent with previous studies by Rorrer and Dorgran²⁹ and Peters et al. who found that $\tau_{\rm e}$ does not depend on the degree of dispersity.

Further insight into the mobility of the chains is obtained by comparing the weight averaged MSD and that of the individual components for the binary and ternary systems, as shown in Figure 3. At early times, there is no difference in the motion of the center beads for the individual components and the motion averaged over all chains. However, at longer times, differences

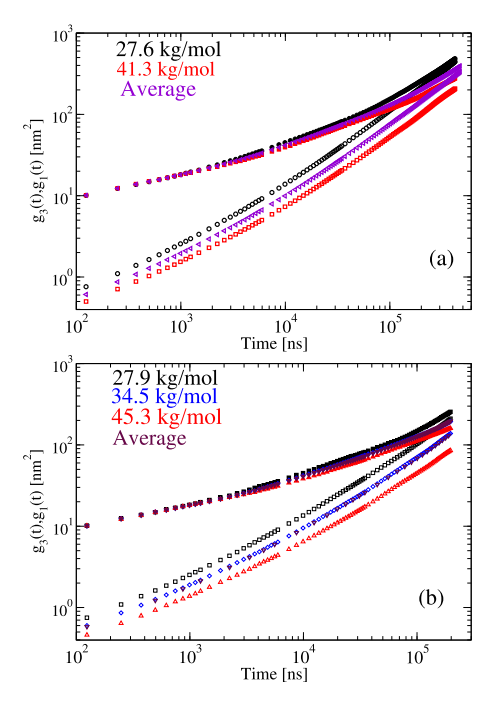


Figure 3. Averaged mean squared displacement of the center of mass $g_3(t)$ (open) and center for CG beads $g_1(t)$ (solid) for weight average (purple) and components for (a) binary distribution and (b) ternary distribution for $\mathcal{D}_{\rm M} = 1.04$.

in the mobility of the shorter and longer chains become evident. These observations are similar to those obtained when probing the shortest and longest chains in the Schulz–Zimm distribution of chain lengths.⁴ In all cases, the shorter chains move significantly faster than the average. For the binary mixture, the shorter chains with M=27.6 kg/mol have a diffusion constant $D_{\rm S}=1.8\times10^{-13}$ m²/s and the longer chains with M=41.3 kg/mol have $D_{\rm L}=8.1\times10^{-14}$ m²/s, compared to the weight averaged diffusion constant $D=1.23\times10^{-13}$ m²/s.

Current results further validate previous studies by Peters et al.4 who showed that in agreement with earlier Monte Carlo simulations of Rorrer and Dorgan, ²⁹ the average chain mobility increases and the terminal time $\tau_{\rm d}$, when the MSD becomes diffusive, decreases as \mathcal{D}_{M} increases. The weight averaged diffusion constant D increases by 50% as $D_{\rm M}$ increases from 1.0 to 1.16 for PE.³³ Results for a uniform melt ($D_{\rm M}$ = 1.0) and the lowest dispersity $D_{\rm M}$ = 1.02 are nearly indistinguishable. At early times, the motion of the inner monomers does not depend on \mathcal{D}_{M} , as all of the chains, even for \mathcal{D}_{M} =1.16, are much longer than the entanglement length for $M_{\rm w} = 35.8$ kg/ mol. Comparing the MSD for the shortest and longest 5% of the chains for the Schulz-Zimm distribution, the shorter chains were observed to move significantly faster than the average as the dispersity increases. In the dispersed melts, the longer chains move faster than in a uniform melt of long chains. This increase in the mobility of the long chains occurs even for low dispersity. This increase in the mobility of the long chains is attributed to constraint release due to the shorter chains. This enhanced mobility is expected to affect the viscoelastic response.

The stress relaxation G(t) for dispersity in the range $D_{\rm M}$ = 1.0–1.16 for the Schulz–Zimm distribution was calculated in two ways: from the stress autocorrelation function shown in Figure 4 and from the stress relaxation after extension shown in

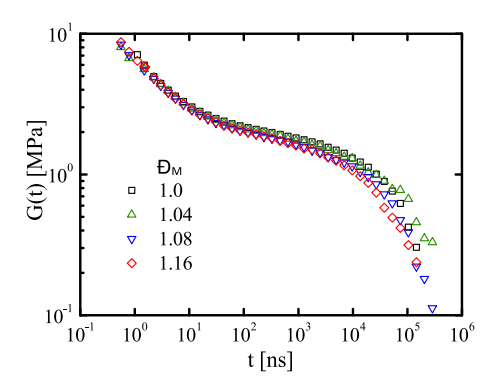


Figure 4. Stress relaxation modulus G(t) using the Green–Kubo formula for Schulz–Zimm distribution with $D_{\rm M}=1.0-1.16$ with $M_{\rm w}=35.8$ kg/mol at 500 K.

Figure 5. As shown in Figure 4, at short times, G(t) decays rapidly as the chains locally relax within their tube,

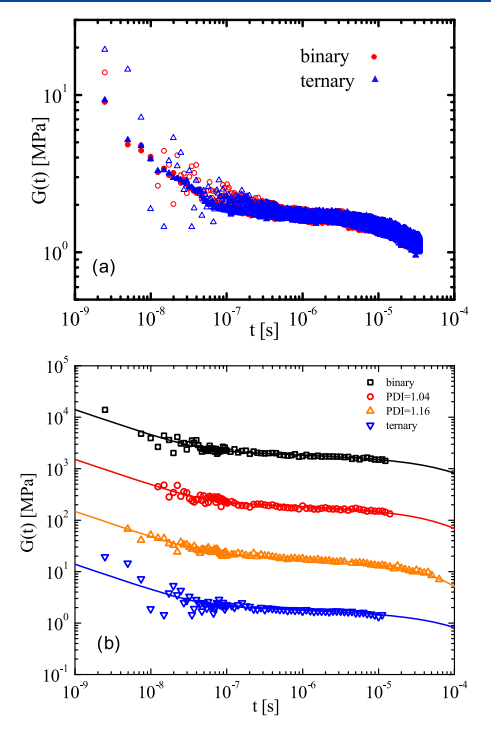


Figure 5. (a) G(t) using the stress–strain formula, eq 1 for strain rates $8.1 \times 10^6/\mathrm{s}$ (open symbols) and $9.0 \times 10^5/\mathrm{s}$ (closed symbols) for binary (circles) and ternary (triangles) blends. (b) G(t) for $D_\mathrm{M} = 1.04$ (red) and 1.16 (orange) for Schulz–Zimm formula, 1.04 binary (black) and 1.04 ternary (blue) for an extension rate of $1.45 \times 10^5/\mathrm{s}$. Lines are the guide to the eye. Results are offset by a factor of 10 for clarity.

independent of \mathcal{D}_{M} . Only after the chains have reached the diffusive regime does G(t) relax to zero at a time τ_{d} , which decreases with increasing \mathcal{D}_{M} . From the results shown in Figure 4, we estimate that the plateau modulus $G_{\mathrm{N}}^0 \sim 1.8-2.0$ MPa, which using the expression $G_{\mathrm{N}}^0 = \frac{4}{5} \frac{\rho RT}{M_{\mathrm{e}}}$ gives an entanglement length of $M_{\mathrm{e}} = 1.1-1.3$ kg/mol, consistent with the experiment. However, much longer chains are needed to obtain a more definitive value for G_{N}^{0} . Currently, such computations are not feasible.

Determination of the stress relaxation function G(t) from fluctuations in the off-diagonal components of the stress tensor usually requires simulations several times the longest relaxation time. An alternative method is to follow the experimental procedure and apply a small strain and measure stress relaxation. Although computationally more efficient than the stress autocorrelation function, the challenge is to apply a strain small enough to be able to reliably measure the stress yet remain in the linear response regime, which we were able to do in this study. Following Hsu and Kremer, 53 we applied a uniaxial strain of $\lambda = 1.2$. Results for G(t) at strain rates of 8.1 \times 10⁶/s and 9.0 \times 10⁵/s are shown in Figure 5a. The results for the two rates are similar except at very early times ($t < \sim 200$ ns). G(t) for the binary, ternary, and SZ distributions with \mathcal{D}_{M} = 1.04 and for the SZ distribution with $D_{\rm M}$ = 1.16 are shown in Figure 5b. We find that the plateau modulus $G_N^0 = 1.8$ MPa in agreement with the results from the stress autocorrelation function, except at early times where the system begins to relax while being extended. At early time, the decay of G(t) depends on the strain rate and differs from that obtained from the autocorrelation function and MSD, presumably due to the finite strain rates used in this approach, while the diffusive times τ_d are comparable for the two methods.

Another way to characterize the viscoelastic response is to measure the shear viscosity η as a function of the shear rate $\dot{\gamma}$. The start-up viscosity as a function of time for $D_{\rm M}=1.04$ and 1.16 is shown in Figure 6a for the three values of the shear rate $\dot{\gamma}$. At early times, after the shear is imposed, there is an overshoot in the shear viscosity, which is independent of the dispersity for the values of $D_{\rm M}$ studied here. The steady-state shear viscosity is shown in Figure 6b for five systems. Over the entire range of accessible shear rates, which are all in the nonlinear regime due to computational limitations, the

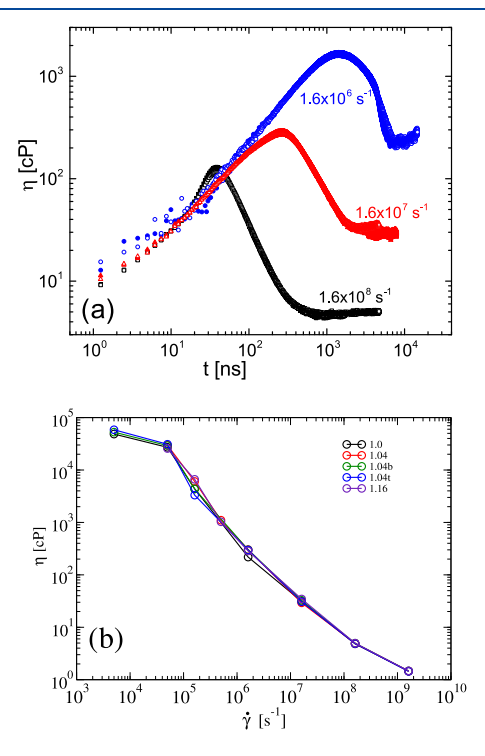


Figure 6. (a) Shear viscosity η as a function of time for the three shear rates for $D_{\rm M}=1.04$ (solid) and 1.16 (open). (b) Shear viscosity η as a function of the strain rate $\dot{\gamma}$ for $M_{\rm w}=35.8$ kg/mol and $D_{\rm M}=1.0$, 1.04 for Schulz–Zimm, binary, and ternary, and 1.16 for Schulz–Zimm.

difference between the five systems is negligible. The fact that η is independent of \mathcal{D}_{M} is consistent with the experimental results of Struglinski and Graessley, who found that the zero shear rate viscosity is essentially independent of \mathcal{D}_{M} over a very large range of dispersity. Accessing the linear regime computationally, where the viscosity is independent of the shear rate remains a challenge. Unfortunately, it is also not possible to determine the strain rate at which shear-thinning begins and study its dependence on \mathcal{D}_{M} . In summary, while the stress relaxation G(t) at long times decays faster as \mathcal{D}_{M} increases, there is no sign of this behavior in the shear viscosity, at least for the range of the shear rates currently accessible computationally.

CONCLUSIONS

Here, using a CG polyethylene model with four CH2 groups per CG bead, we have studied the effects of chain length dispersity on chain mobility and stress relaxation at the onset of dispersity. The range of dispersity studied covers the lowest accessible experimentally by polymer synthesis routes. This study found that weight averaged chain mobility increases as dispersity increases but does not depend on the form of the distribution for the narrow distributions studied here. The increased diffusion of the shorter chains results in constraint release for the longer chains, leading to the faster motion of the longer chains in the dispersed melts than in a uniform melt of the longer chains. On the entanglement time scale τ_e , both the MSD and the stress autocorrelation function $G(\tau_e)$ are independent of the dispersity index \mathcal{D}_{M} . At longer times, the stress autocorrelation function decreases faster with increasing dispersity, consistent with the decrease in the terminal relaxation time $\tau_{\rm d}$. Further simulations with much larger $D_{\rm M}$ are currently underway with the long-term goal of accessing the linear regime.

AUTHOR INFORMATION

Corresponding Author

Gary S. Grest — Sandia National Laboratories, Albuquerque, New Mexico 87185, United States; o orcid.org/0000-0002-5260-9788; Email: gsgrest@sandia.gov

Authors

Brandon L. Peters – Sandia National Laboratories, Albuquerque, New Mexico 87185, United States

K. Michael Salerno – U. S. Army Research Laboratory, Aberdeen, Maryland 21005, United States

Ting Ge − Department of Chemistry and Biochemistry, University of South Carolina, Columbia, South Carolina 29208, United States; orcid.org/0000-0003-2456-732X

Dvora Perahia — Department of Chemistry and Department of Physics and Astronomy, Clemson University, Clemson, South Carolina 29634, United States; ⊙ orcid.org/0000-0002-8486-8645

Complete contact information is available at: https://pubs.acs.org/10.1021/acs.macromol.0c01403

Notes

The authors declare no competing financial interest.

■ ACKNOWLEDGMENTS

D.P. kindly acknowledged NSF DMR1905407 for partial support. This work was supported by Laboratory Directed

Research and Development Program at Sandia National Laboratories. This work was performed, in part, at the Center for Integrated Nanotechnologies, an Office of Science User Facility operated for the U.S. Department of Energy (DOE) Office of Science. Sandia National Laboratories is a multimission laboratory managed and operated by the National Technology and Engineering Solutions of Sandia, LC, a wholly owned subsidiary of Honeywell International, Inc., for the U.S. Department of Energy's National Nuclear Security Administration under contract no. DE-NA-0003525. The views expressed in the article do not necessarily represent the views of the U.S. DOE or the United States Government.

REFERENCES

- (1) Rubinstein, M.; Colby, R. H. *Polymer Physics*; Oxford University Press: New York, 2003.
- (2) Matyjaszewski, K.; Xia, J. Atom transfer radical polymerization. *Chem. Rev.* **2001**, *101*, 2921–2990.
- (3) Chiefari, J.; Chong, Y.; Ercole, F.; Krstina, J.; Jeffery, J.; Le, T. P.; Mayadunne, R. T.; Meijs, G. F.; Moad, C. L.; Moad, G.; Rizzardo, E.; Thang, S. Living free-radical polymerization by reversible addition-fragmentation chain transfer: the RAFT process. *Macromolecules* 1998, 31, 5559–5562.
- (4) Peters, B. L.; Salerno, K. M.; Ge, T.; Perahia, D.; Grest, G. S. Effect of Chain Length Dispersity on the Mobility of Entangled Polymers. *Phys. Rev. Lett.* **2018**, *121*, No. 057802.
- (5) Struglinski, M. J.; Graessley, W. W. Effects of polydispersity on the linear viscoelastic properties of entangled polymers. 1. Experimental observations for binary mixtures of linear polybutadiene. *Macromolecules* **1985**, *18*, 2630–2643.
- (6) Wasserman, S.; Graessley, W. Effects of polydispersity on linear viscoelasticity in entangled polymer melts. *J. Rheol.* **1992**, *36*, 543–572.
- (7) Doi, M.; Edwards, S. F. The Theory of Polymer Dynamics; Clarendon Press: Oxford, 1988.
- (8) Graessley, W. W.; Struglinski, M. J. Effects of polydispersity on the linear viscoelastic properties of entangled polymers. 2. Comparison of viscosity and recoverable compliance with tube model predictions. *Macromolecules* **1986**, *19*, 1754–1760.
- (9) Schieber, J. D.; Curtiss, C. F.; Bird, R. B. Kinetic theory of polymer melts. 7. Polydispersity effects. *Ind. Eng. Chem. Fundam.* **1986**, 25, 471–475.
- (10) Doi, M.; Graessley, W.; Helfand, E.; Pearson, D. Dynamics of polymers in polydisperse melts. *Macromolecules* **1987**, 20, 1900–1906.
- (11) Rubinstein, M.; Colby, R. H. Self-consistent theory of polydisperse entangled polymers: Linear viscoelasticity of binary blends. *J. Chem. Phys.* **1988**, 89, 5291–5306.
- (12) Tsenoglou, C. Molecular weight polydispersity effects on the viscoelasticity of entangled linear polymers. *Macromolecules* **1991**, *24*, 1762–1767.
- (13) Milner, S. T. Relating the shear-thinning curve to the molecular weight distribution in linear polymer melts. *J. Rheol.* **1996**, *40*, 303–315.
- (14) Wang, S.; Wang, S.-Q.; Halasa, A.; Hsu, W.-L. Relaxation dynamics in mixtures of long and short chains: Tube dilation and impeded curvilinear diffusion. *Macromolecules* **2003**, *36*, 5355–5371.
- (15) Léonardi, F.; Majeste, J.-C.; Allal, A.; Marin, G. Rheological models based on the double reptation mixing rule: the effects of a polydisperse environment. *J. Rheol.* **2000**, *44*, 675–692.
- (16) Cassagnau, P.; Montfort, J.; Marin, G.; Monge, P. Rheology of polydisperse polymers: relationship between intermolecular interactions and molecular weight distribution. *Rheol. Acta* **1993**, 32, 156–167.
- (17) Baschnagel, J.; Paul, W.; Tries, V.; Binder, K. Statics and dynamics of bidisperse polymer melts: A Monte Carlo study of the bond-fluctuation model. *Macromolecules* **1998**, *31*, 3856–3867.

- (18) Masubuchi, Y.; Watanabe, H.; Ianniruberto, G.; Greco, F.; Marrucci, G. Comparison among slip-link simulations of bidisperse linear polymer melts. *Macromolecules* **2008**, *41*, 8275–8280.
- (19) Martínez-Veracoechea, F. J.; Escobedo, F. A. Lattice Monte Carlo simulations of the gyroid phase in monodisperse and bidisperse block copolymer systems. *Macromolecules* **2005**, *38*, 8522–8531.
- (20) Barsky, S. Molecular dynamics study of diffusion in bidisperse polymer melts. *J. Chem. Phys.* **2000**, *112*, 3450–3456.
- (21) Picu, R.; Rakshit, A. Coarse grained model of diffusion in entangled bidisperse polymer melts. *J. Chem. Phys.* **2007**, 127, No. 144909.
- (22) Read, D.; Jagannathan, K.; Sukumaran, S.; Auhl, D. A full-chain constitutive model for bidisperse blends of linear polymers. *J. Rheol.* **2012**, *56*, 823–873.
- (23) Barsky, S.; Slater, G. W. A nonequilibrium molecular dynamics simulation of the time-dependent orientational coupling between long and short chains in a bimodal polymer melt upon uniaxial stretching. *Macromolecules* **1999**, *32*, 6348–6358.
- (24) Harmandaris, V. A.; Mavrantzas, V. G.; Theodorou, D. N. Atomistic molecular dynamics simulation of polydisperse linear polyethylene melts. *Macromolecules* **1998**, *31*, 7934–7943.
- (25) Mavrantzas, V. G.; Boone, T. D.; Zervopoulou, E.; Theodorou, D. N. End-bridging Monte Carlo: A fast algorithm for atomistic simulation of condensed phases of long polymer chains. *Macromolecules* 1999, 32, 5072–5096.
- (26) Pant, P. V. K.; Theodorou, D. N. Variable connectivity method for the atomistic Monte Carlo simulation of polydisperse polymer melts. *Macromolecules* **1995**, 28, 7224–7234.
- (27) Daoulas, K. C.; Terzis, A. F.; Mavrantzas, V. G. Variable connectivity methods for the atomistic Monte Carlo simulation of inhomogeneous and/or anisotropic polymer systems of precisely defined chain length distribution: tuning the spectrum of chain relative chemical potentials. *Macromolecules* **2003**, *36*, 6674–6682.
- (28) Rorrer, N. A.; Dorgan, J. R. Effects of polydispersity on confined homopolymer melts: A Monte Carlo study. *J. Chem. Phys.* **2014**, *141*, No. 214905.
- (29) Rorrer, N. A.; Dorgan, J. R. Finding the missing physics: Mapping polydispersity into lattice-based simulations. *Macromolecules* **2014**, *47*, 3185–3191.
- (30) Dorgan, J. R.; Rorrer, N. A. Molecular scale simulation of homopolymer wall slip. *Phys. Rev. Lett.* **2013**, *110*, No. 176001.
- (31) Rorrer, N. A.; Dorgan, J. R. Molecular-scale simulation of cross-flow migration in polymer melts. *Phys. Rev. E* **2014**, *90*, No. 052603.
- (32) Li, S.-J.; Xie, S.-J.; Li, Y.-C.; Qian, H.-J.; Lu, Z.-Y. Influence of molecular-weight polydispersity on the glass transition of polymers. *Phys. Rev. E* **2016**, 93, No. 012613.
- (33) Salerno, K. M.; Agrawal, A.; Perahia, D.; Grest, G. S. Resolving Dynamic Properties of Polymers through Coarse-Grained Computational Studies. *Phys. Rev. Lett.* **2016**, *116*, No. 058302.
- (34) Salerno, K. M.; Agrawal, A.; Peters, B. L.; Perahia, D.; Grest, G. S. Dynamics in entangled polyethylene melts. *Eur. Phys. J.: Spec. Top.* **2016**, 225, 1707–1722.
- (35) Peters, B. L.; Salerno, K. M.; Agrawal, A.; Perahia, D.; Grest, G. S. Coarse Grained Modeling of Polyethylene Melts: Effect on Dynamics. *J. Chem. Theory Comput.* **2017**, *13*, 2890–2896.
- (36) Zimm, B. H. The scattering of light and the radial distribution function of high polymer solutions. *J. Chem. Phys.* **1948**, *16*, 1093–1099.
- (37) Hiemenz, P. C.; Lodge, T. P. Polymer Chemistry; CRC Press, 2007.
- (38) Salerno, K. M.; Bernstein, N. Persistence Length, End-to-End Distance, and Structure of Coarse-Grained Polymers. *J. Chem. Theory Comput.* **2018**, *14*, 2219–2229.
- (39) Padding, J. T.; Briels, W. J. Uncrossability constraints in mesoscopic polymer melt simulations: Non-Rouse behavior of C120H242. J. Chem. Phys. 2001, 115, 2846–2859.
- (40) Padding, J. T.; Briels, W. J. Time and length scales of polymer melts studied by coarse-grained molecular dynamics simulations. *J. Chem. Phys.* **2002**, *117*, 925–943.

- (41) Jorgensen, W. L.; Madura, J. D.; Swenson, C. J. Optimized intermolecular potential functions for liquid hydrocarbons. *J. Am. Chem. Soc.* **1984**, *106*, 6638–6646.
- (42) Jorgensen, W. L.; Maxwell, D. S.; Tirado-Rives, J. Development and Testing of the OPLS All-Atom Force Field on Conformational Energetics and Properties of Organic Liquids. *J. Am. Chem. Soc.* **1996**, 118, 11225–11236.
- (43) Siu, S. W. I.; Pluhackova, K.; Böckmann, R. A. Optimization of the OPLS-AA Force Field for Long Hydrocarbons. *J. Chem. Theory Comput.* **2012**, *8*, 1459–1470.
- (44) Fetters, L. J.; Lohse, D. J.; Richter, D.; Witten, T. A.; Zirkel, A. Connection between Polymer Molecular Weight, Density, Chain Dimensions, and Melt Viscoelastic Properties. *Macromolecules* **1994**, 27, 4639–4647.
- (45) Fetters, L. J.; Lohse, D. J.; Milner, S. T.; Graessley, W. W. Packing Length Influence in Linear Polymer Melts on the Entanglement, Critical, and Reptation Molecular Weights. *Macromolecules* **1999**, 32, 6847–6851.
- (46) Vega, J. F.; Rastogi, S.; Peters, G. W. M.; Meijer, H. E. H. Rheology and reptation of linear polymers. Ultrahigh molecular weight chain dynamics in the melt. *J. Rheol.* **2004**, *48*, 663–678.
- (47) Plimpton, S. Fast Parallel Algorithms for Short-Range Molecular Dynamics. *J. Comput. Phys.* **1995**, *117*, 1–19.
- (48) Auhl, R.; Everaers, R.; Grest, G. S.; Kremer, K.; Plimpton, S. J. Equilibration of long chain polymer melts in computer simulations. *J. Chem. Phys.* **2003**, *119*, 12718–12728.
- (49) Depa, P.; Chen, C.; Maranas, J. K. Why are coarse-grained force fields too fast? A look at dynamics of four coarse-grained polymers. *J. Chem. Phys.* **2011**, *134*, No. 014903.
- (50) Lyubimov, I. Y.; Guenza, M. G. Theoretical reconstruction of realistic dynamics of highly coarse-grained cis-1,4-polybutadiene melts. *J. Chem. Phys.* **2013**, 138, No. 12A546.
- (51) Harmandaris, V. A.; Kremer, K. Dynamics of polystyrene melts through hierarchical multiscale simulations. *Macromolecules* **2009**, *42*, 791–802.
- (52) Fritz, D.; Koschke, K.; Harmandaris, V. A.; van der Vegt, N. F. A.; Kremer, K. Multiscale modeling of soft matter: scaling of dynamics. *Phys. Chem. Chem. Phys.* **2011**, *13*, 10412–10420.
- (53) Hsu, H.-P.; Kremer, K. Static and dynamic properties of large polymer melts in equilibrium. *J. Chem. Phys.* **2016**, 144, No. 154907. (54) Treloar, L. R. G. *The Physics of Rubber Elasticity*; Oxford University Press: USA, 1975.
- (55) Kremer, K.; Grest, G. S. Dynamics of entangled linear polymer melts: A molecular-dynamics simulation. *J. Chem. Phys.* **1990**, 92, 5057–5086.
- (56) Hoover, W. G. Canonical dynamics: Equilibrium phase-space distributions. *Phys. Rev. A* **1985**, *31*, 1695–1697.
- (57) Evans, D.; Morriss, G. Statistical Mechanics of Nonequilibrium Liquids Academic *New York* 1990, 8.
- (58) Tuckerman, M. E.; Mundy, C. J.; Balasubramanian, S.; Klein, M. L. Modified nonequilibrium molecular dynamics for fluid flows with energy conservation. *J. Chem. Phys.* **1997**, *106*, 5615–5621.
- (59) Hou, J.-X. Note Determine entanglement length through monomer mean-square displacement. *J. Chem. Phys. A* **2017**, *146*, No. 026101.